The Planck mission

C. R. Lawrence*

Jet Propulsion Laboratory, California Institute of Technology, Pasadena, CA

ABSTRACT

Planck, scheduled for launch in 2007, will be the third space mission to observe the cosmic microwave background (CMB). Two cryogenic instruments and an off-axis telescope will provide an unprecedented combination of sensitivity, angular resolution, and frequency coverage. Planck is designed to measure the temperature anisotropies of the CMB to limits set not by the instruments, but rather by the Universe itself. In addition, it will measure the E-type polarization of the CMB, and provide all-sky surveys at nine frequencies between 30 and 857 GHz.

Keywords: Cosmic microwave background, all-sky surveys, cryogenics, infrared telescopes, radiometers, bolometers

1. OVERVIEW OF THE MISSION

Planck is the third Medium-Sized Mission (M3) of ESA's Horizon 2000 Scientific Programme (see also Refs. 1–3, this volume), and is named in honor of Max Planck (1858-1947), who first calculated the spectrum of radiation in equilibrium with matter at a given temperature. The primary scientific goal of Planck is to measure the temperature anisotropy of the cosmic microwave background (CMB) to fundamental limits set by the Universe itself.

Planck will be the third space mission to observe the anisotropy of the CMB, following COBE (launched in 1989) and MAP (launched in 2001 and now flying). It is scheduled for launch in 2007, and will share an Ariane 5 rocket with the ESA Cornerstone mission Herschel[4–11]. Figure 1 shows Planck and Herschel in the Ariane shroud, and the main components of Planck. Following launch, Planck and Herschel will separate from the rocket and fly independently to L_2, the second Lagrangian point of the Earth-Sun system, approximately 1.6×10^6 km from the Earth along the anti-Sun line (Figure 2). Planck will be injected into a non-deterministic Lissajous orbit around L_2, approximately 400,000 km in radius. The gravitational potential at L_2 is saddle-shaped, and small station-keeping maneuvers will be required every few weeks to maintain the orbit.

Planck will rotate at 1 rpm about its long axis, with the spin axis pointed at the Sun. The solar panel is then face-on to the Sun, and shadows the rest of the spacecraft. This strategy minimises potentially confusing signals due to thermal fluctuations and straylight entering the detectors through the far sidelobes. The solar panel shields the spacecraft not only from the Sun, but also from the Earth and the Moon, which lie close to the Sun as seen from L_2. Communications with Earth are handled with a fixed antenna on the solar panel pointed along the spin axis. The beam is wide enough to cover the Earth as it moves with respect to the Sun due to the Lissajous spacecraft orbit around L_2.

The thermal design of Planck is one of its most important aspects. To achieve the necessary sensitivity, the Planck instruments must operate at cryogenic temperatures. The Low Frequency Instrument[1] (LFI) is based on transistor amplifiers cooled to 20 K by a hydrogen sorption cooler. The High Frequency Instrument[2] (HFI) is based on bolometers cooled to 0.1 K by a chain of three coolers[3]: the sorption cooler provides precooling for a 4-K helium Joule-Thomson cooler, which in turn provides precooling for a ^{3}He–^{4}He dilution cooler.

* charles.lawrence@jpl.nasa.gov; 818 642 1784; M/S 169-327, JPL, 4800 Oak Grove Drive, Pasadena, CA 91109

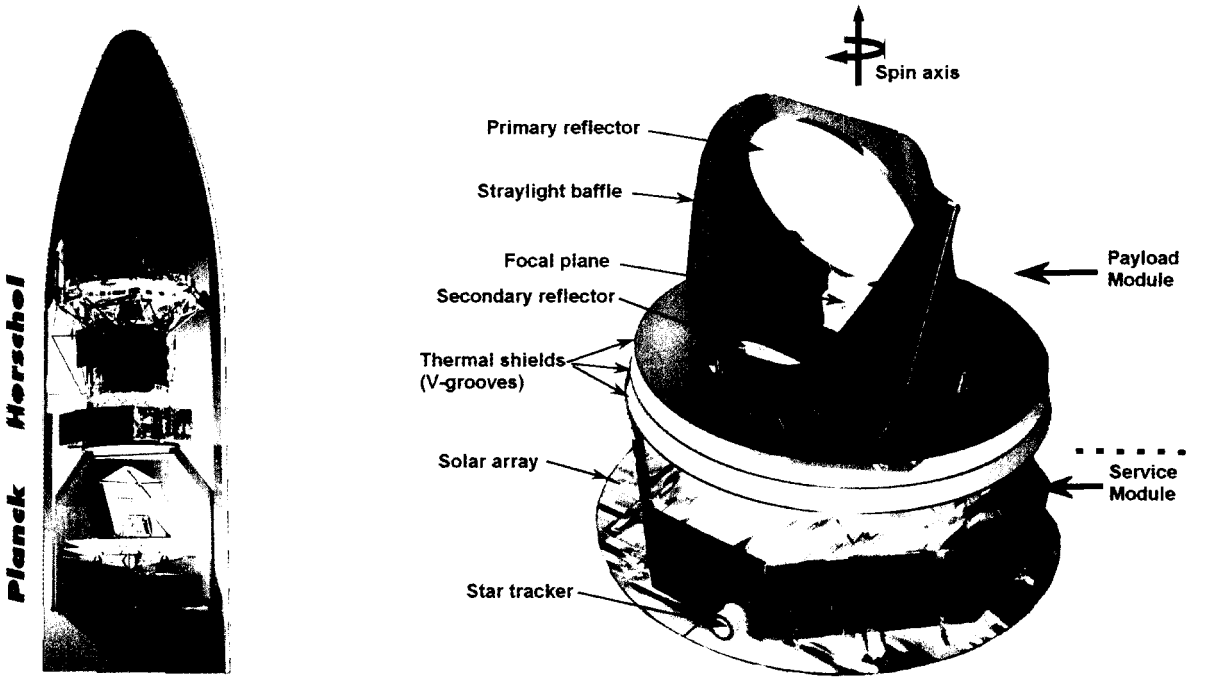

FIG 1.—*Left-hand panel:* Planck and Herschel in the Ariane 5 fairing. The two spacecraft are mounted independently to the rocket. *Right-hand panel:* The main elements of Planck. The off-axis telescope cools radiatively to $< 50\,\mathrm{K}$; three large "V-groove radiators" provide thermal isolation between the warm service module and the cold instruments and telescope. The solar panel is circular and fixed to the bottom of the service module.

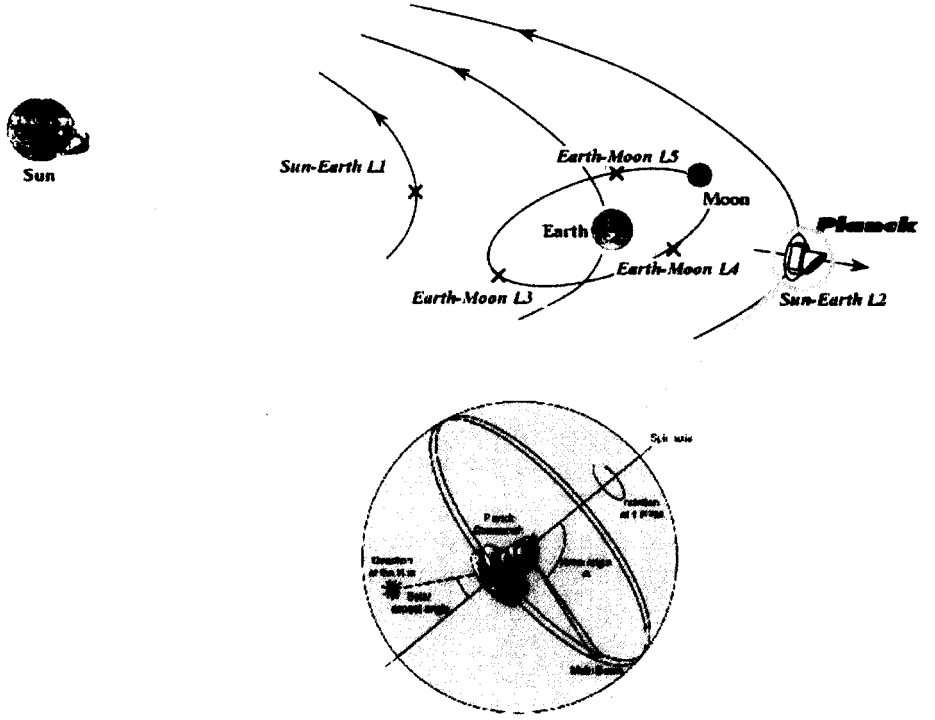

FIG 2Planck orbit at the Earth-Sun L_2 point. Spinning at 1 rpm with its spin axis pointed near the Sun, Planck will scan nearly great circles on the sky, covering the entire sky every six months.

The solar panel (on the bottom in Figure 1) is the hottest part of Planck, while the telescope and straylight baffle are the coldest. The nominal temperature of the service module is 270 K. The temperatures of the V-grooves are nominally 160 K, 100 K, and 55 K. The V-groove geometry provides highly efficient radiative coupling with cold space. All of the components attached between the service module and the instruments (e.g., LFI waveguides, sorption cooler gas pipes, struts supporting the payload) are heat sunk to the V-grooves, which as a result intercept and radiate away heat that would otherwise represent a large conductive parasitic load from the warm parts of the spacecraft on the cold parts. The V-grooves also provide highly efficient radiative isolation of warm and cold parts. The thermal design of Planck, with its careful separation and isolation of warm and cold parts, its agressive use of radiative cooling, and its cryogenic instruments, has much in common with that of SIRTF[12–14], but with the added advantage that the warmest part of Planck, the solar panel, is furthest from the cold parts.

A blackbody spectrum is characterized by a single parameter, its temperature. If the CMB were the only radiation observed by Planck, observations at only a single observing frequency would be required. Unfortunately (from the CMB perspective!), everything else in the Universe comes between us and the CMB. Planck must therefore be able to separate the CMB from foreground emission. Figure 3 shows the brightness temperature (i.e., Rayleigh-Jeans or antenna temperature) of CMB fluctuations as a function of frequency, compared to that of the most important foregrounds. The logarithmically-spaced Planck frequency bands are shaded. LFI observes the four lowest; HFI observes the six highest. Both LFI and HFI observe a band centered at 100 GHz. Simulations show that this broad frequency coverage will enable separation of the CMB from foregrounds with high accuracy.

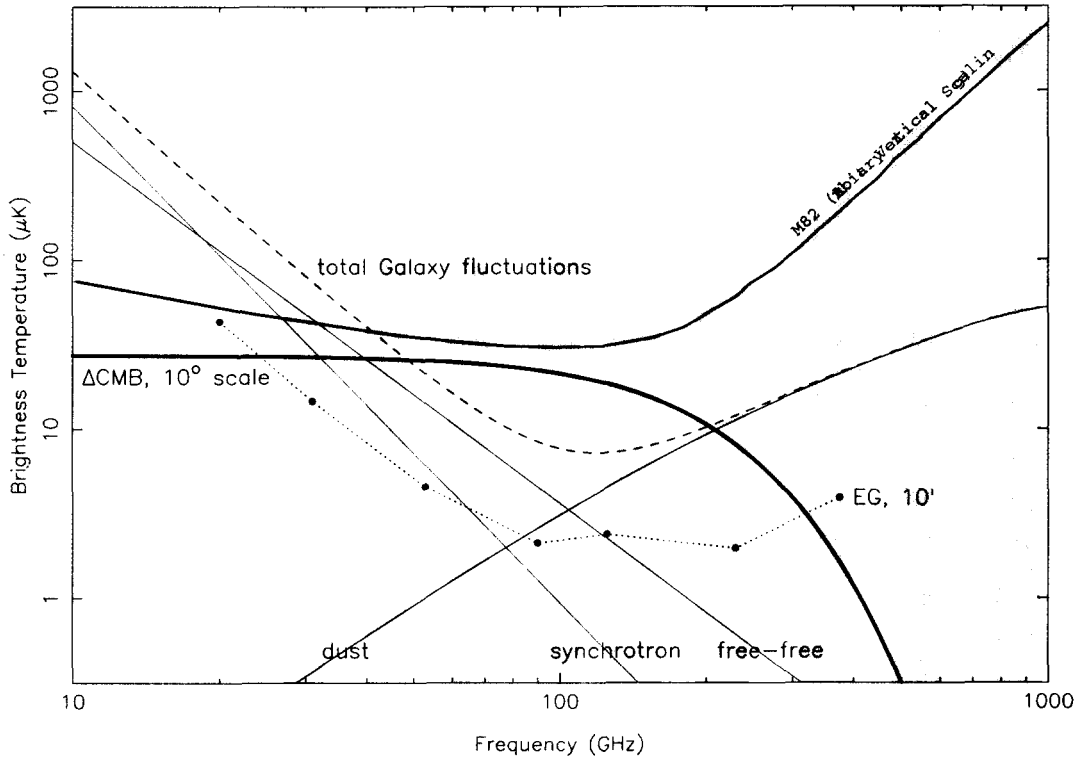

FIG 3.— The Planck frequency bands and the frequency spectra of the dominant Galactic foregrounds, synchrotron, free-free, and dust emission. Also shown are the expected level of CMB fluctuations on a 10° scale, and, as a light dashed line (EG), the expected level of fluctuations introduced by all foreground radio sources on a 10′ angular scale.

Table 1 lists the main performance parameters of Planck (see Refs. 1–3 for details). Both instruments use large arrays of state-of-the-art detectors to achieve the performance indicated. The bolometers on Planck will operate within a factor of two of background-limited performance, and the amplifiers will operate at 5–7 times

the quantum limit. LFI and HFI will be the most sensitive instruments ever built for their respective frequency ranges.

TABLE 1

PLANCK INSTRUMENT CHARACTERISTICS

	LFI				HFI					
INSTRUMENT CHARACTERISTIC										
Detector Technology	HEMT radiometer arrays				Bolometer arrays					
Center Frequency [GHz]	30	44	70	100	100	143	217	353	545	857
Number of Detectors	4	6	12	24	4	12	12	6	8	6
Bandwidth ($\Delta\nu/\nu$)	0.2	0.2	0.2	0.2	0.33	0.33	0.33	0.33	0.33	0.33
Angular Resolution (arcmin)	33	24	14	10	9.2	7.1	5.0	5.0	5.0	5.0
ΔT per pixel (Stokes I)[a] [μK]	5.5	7.4	13	21	5.5	6.0	13	40	400	18300
ΔT per pixel (Stokes Q & U)[a] [μK]	7.7	10	18	30	...	11	27	81	...	...
Sensitivity to unresolved sources [mJy][b]	15	23	32	49	7.2	7.5	10	20	38	44

[a] 1σ goal noise, averaged over the sky for 12 months integration, per square pixels whose sides are given in the row "Angular Resolution".

[b] 1σ instrumental sensitivity to unresolved sources. No account is taken of confusion or other confusing sources of radiation (e.g., in this case, intrinsic CMB anisotropies).

Both COBE and MAP measured temperature differences between two spots separated by a large angle on the sky. This differential technique is extremely effective in rejecting many types of spurious signals that can contaminate CMB data. Planck uses a different strategy, measuring directly the temperature of the sky as it scans. The reason is straightforward. Even with detectors close to fundamental performance limits, the overall noise level, angular resolution, and frequency coverage that Planck must achieve to realize its science goals require a very large number of cryogenic detectors. The Planck scheme allows a much higher number of detectors for a given overall size of the mission than the COBE/MAP scheme. The price for this high performance is paid in the complexity of the data analysis, where strong non-diagonality of the noise correlation matrix must be dealt with, and in the extra care that must be given in both hardware design and data analysis to the control of systematic errors.

2. THE COSMIC MICROWAVE BACKGROUND

The aims of Planck are unique among experiments designed to measure temperature and polarization anisotropies of the CMB. Planck has been designed to produce maps of the temperature and polarization anisotropies at 5′ resolution, with microkelvin sensitivity per resolution element, over the entire sky. The small scale features in the CMB sky provide a 'cosmic fingerprint' of the Universe. The precise statistics of the CMB anisotropies allow tests of the ultra-early Universe and the determination of cosmological parameters to extraordinarily high precision.

Temperature anisotropies in simple inflationary models arise from two distinct physical processes:

Potential Fluctuations in the Early Universe: On angular scales $\theta \gtrsim 1°$, temperature anisotropies measure fluctuations in the gravitational potential along different lines of sight, $\Delta T/T_0 \approx \frac{1}{3}\Delta\phi/c^2$. This is often called the Sachs-Wolfe effect[15] and is of particular importance because it links temperature anisotropies directly with potential fluctuations generated in the early Universe.

Sound Waves Prior to Recombination: In the standard hot Big Bang model, the Universe is highly ionised until a redshift $z_R \sim 1100$, the so-called recombination epoch about 300,000 years after the Big Bang, when protons and electrons combine at a temperature of $\sim 3000\,\mathrm{K}$ to make hydrogen atoms. Prior to this epoch, photons are tightly coupled to the electrons by Thomson scattering, but once recombination is complete the Universe becomes transparent to radiation and CMB photons propagate towards us along geodesics, almost unimpeded

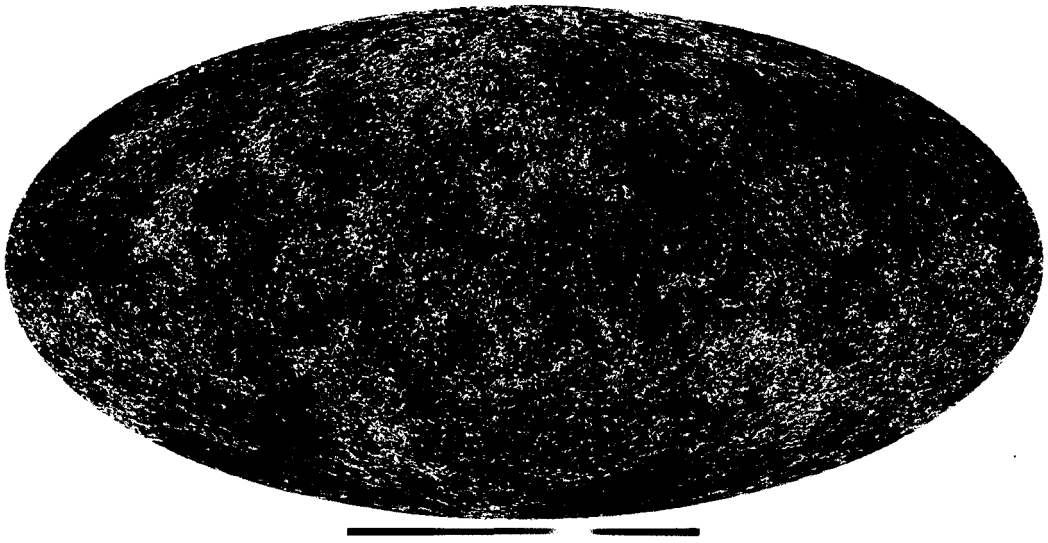

FIG 4.—Simulation of the temperature anisotropies in the CMB sky in inflationary CDM models. The original image has 50 million pixels, appropriate for the Planck angular resolution of 5′; detail is lost in the reproduction. A Mollweide equal-area projection is used.

by matter. The original 3000-K blackbody radiation is redshifted by the 1100-fold expansion of the Universe into the 2.726 K blackbody we observe today. Maps of the CMB therefore provide us with a picture of irregularities at the 'last scattering surface' when the Universe was about 300,000 years old. Small-scale fluctuations in the matter-radiation fluid at this epoch were causally connected and oscillated like sound waves. The small scale structure in the CMB (evident in Figure 4) is a consequence of these oscillations. The characteristic scale of this structure at $\theta \approx 1^\circ$ (corresponding to a prominent acoustic peak in the CMB power spectrum at multipoles of $\ell \sim 200$ as shown several figures below) indicates the maximum distance that a sound wave can travel up to the time of recombination. Accurate measurements of the temperature (and polarization) anisotropies on small angular scales thus provide information on the sound speed at the time of recombination and hence on the matter content of the Universe. Furthermore, the relation between physical distance and angular separations on the sky provides information on the geometry of the Universe. The statistics of the temperature anisotropies can therefore be used to derive fundamental parameters that define our Universe, such as the spatial curvature, Hubble constant H_0, and baryon and dark matter densities. *One of the principal goals of Planck is to determine these fundamental parameters to unprecedented accuracies of better than 1%.*

The temperature anisotropies of the sky can be expanded in spherical harmonics,

$$\frac{\Delta T}{T_0} = \sum_{\ell m} a_{\ell m} Y_{\ell m}(\theta, \phi).$$

A wide class of models of the early Universe predict that the temperature anisotropies obey Gaussian statistics. If this is the case, then all of the statistical properties of the temperature anisotropies can be computed from a single function, the *temperature power spectrum*

$$C_\ell^T = \langle |a_{\ell m}|^2 \rangle,$$

as a function of the multipole index ℓ. More generally, since the CMB anisotropies are expected to be linearly polarized, the temperature and polarization anisotropies in Gaussian models can be characterised by four power spectra, C^T, C^E, C^B, C^X, describing the temperature anisotropies, E- and B-type polarization, and the temperature-polarization cross correlations.

Because of the ubiquity of Gaussian theories, and the lack of any convincing experimental evidence of non-Gaussianity, a large amount of effort has gone into measuring and interpreting the CMB temperature power

spectrum. Accordingly, the measurement of the CMB temperature and polarization power spectra to high precision up to multipoles $\ell \gtrsim 2500$ is one of the primary scientific goals of the Planck mission. However, Planck is not simply an experiment designed to measure power spectra to high precision. Planck's sensitivity, angular resolution, and frequency coverage mean that it is well-suited to detecting small departures from Gaussianity and unusual rare events. The Gaussian assumption is such a critical feature of theoretical models that it needs to be tested experimentally to high precision. This will be achieved by Planck. Non-gaussianity can arise in a variety of ways, including multi-field inflation models and from cosmic defects. Clearly, the detection of even a small degree of non-Gaussianity in the CMB would have potentially revolutionary implications for early Universe physics.

Shortly after the discovery of primordial CMB anisotropies in 1992 by the COBE satellite[16], various analyses demonstrated that the COBE observations could be used to set crude constraints on the amplitude and spectral index of scalar fluctuations. However, with higher angular resolution, greater sensitivity, and the capability to measure polarization, it is possible to constrain a much larger number of cosmological parameters, including the geometry of the the Universe, the dark matter and baryonic densities, the possible contribution of tensor modes, the existence of quintessence, and massive neutrinos. The tremendous potential of CMB anisotropies to revolutionize cosmology has been demonstrated convincingly by subsequent ground based and balloon borne experiments. Figure 5, adapted from Ref. 17, shows a summary of the results of current CMB anisotropy measurements. Note that the temperature fluctuation ΔT_ℓ is related to the power spectrum C_ℓ^T according to

$$\Delta T_\ell = T_0 \left[\frac{\ell(\ell+1)}{2\pi} C_\ell^T \right]^{1/2} .$$

The position of the first prominent acoustic peak in the CMB power spectrum at $\ell \sim 200$ provides extremely strong evidence that the Universe is spatially flat. Evidence exists for up to five acoustic peaks. The presence of multiple, coherent, acoustic peaks is powerful evidence that the primordial fluctuations were generated during an inflationary-like phase in the early Universe.

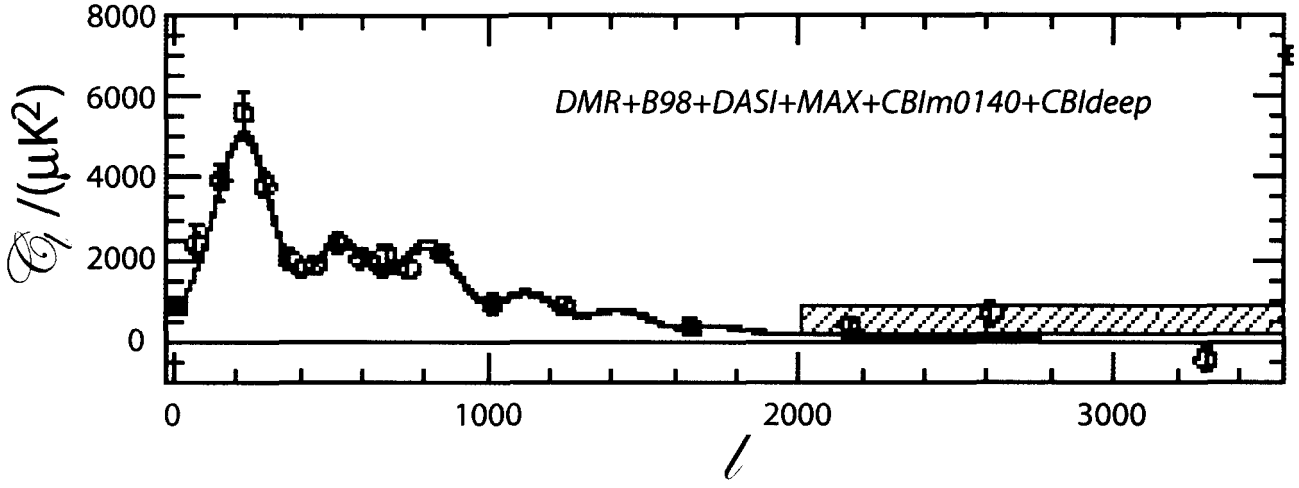

FIG 5.—Current best estimate of the power spectrum of CMB temperature fluctuations, from Ref. 17, based on a combination of data from the COBE DMR, Boomerang, DASI, Maxima, and CBI experiments. The abscissa is multipole ℓ in a spherical harmonic expansion. The peak of the power spectrum, at $\ell \approx 200$, corresponds to an angular scale of about 1°. The ordinate is the standard power spectrum C_ℓ, which corresponds to $(\Delta T)^2$, where ΔT is in microkelvin. The curve is a "best fit" model with $\{\Omega_{\rm tot} = 1.0, \Omega_\Lambda = 0.6, \Omega_b h^2 = 0.02, \Omega_{\rm cdm} h^2 = 0.12, n_s = 0.975$, and $\tau_C = 0.025$.

In fact, detailed analyses of these data show that they are consistent with the *simplest* cold dark matter (CDM) dominated inflationary models. It is remarkable that such a simple model is consistent with the data. It is equally remarkable, however, that the physical basis for Ω_Λ of order unity is a complete mystery!

The NASA MAP satellite launched last year will improve significantly on these results and, in addition, should provide the first all-sky polarization maps of the CMB. Various ground based and balloon borne experiments designed to measure polarization are expected to yield results within the next two years.

3. THE NEED FOR PLANCK

With all of these new results on the CMB and forthcoming experiments, is there still a strong case for CMB science with Planck? What new physics might we hope to learn? Figure 6 shows simulated power spectra for experiments with the characteristics of MAP and Planck. Planck will be able to measure nearly an order of magnitude more multipoles than MAP with SNR > 1. But is this information important? Figure 7 (plotted for the same ℓ range, but logarithmically so that the lower ℓs are expanded for clarity) illustrates it is. The top panels of Figure 7 show C_ℓ for two nearly scale invariant adiabatic models, specified by the following parameters:

- n_s and n_t, the spectral indices for the scalar and tensor components;
- Q_{10}, the amplitude of the scalar component, specified by the amplitude of the $\ell = 10$ multipole relative to that measured by COBE;
- $r_2 \equiv C_2^t/C_2^s$, the ratio of the tensor and scalar amplitudes;
- $\omega_{\rm cdm} = \Omega_{\rm cdm}h^2$ and $\omega_{\rm b} = \Omega_{\rm b}h^2$, the physical densities of cold dark matter and baryons, respectively; and
- $\Omega_{\rm k} \equiv 1 - \Omega_{\rm b} - \Omega_{\rm cdm} - \Omega_\Lambda$, the curvature of the Universe, where Ω_Λ is the cosmological density parameter contributed by a cosmological constant.

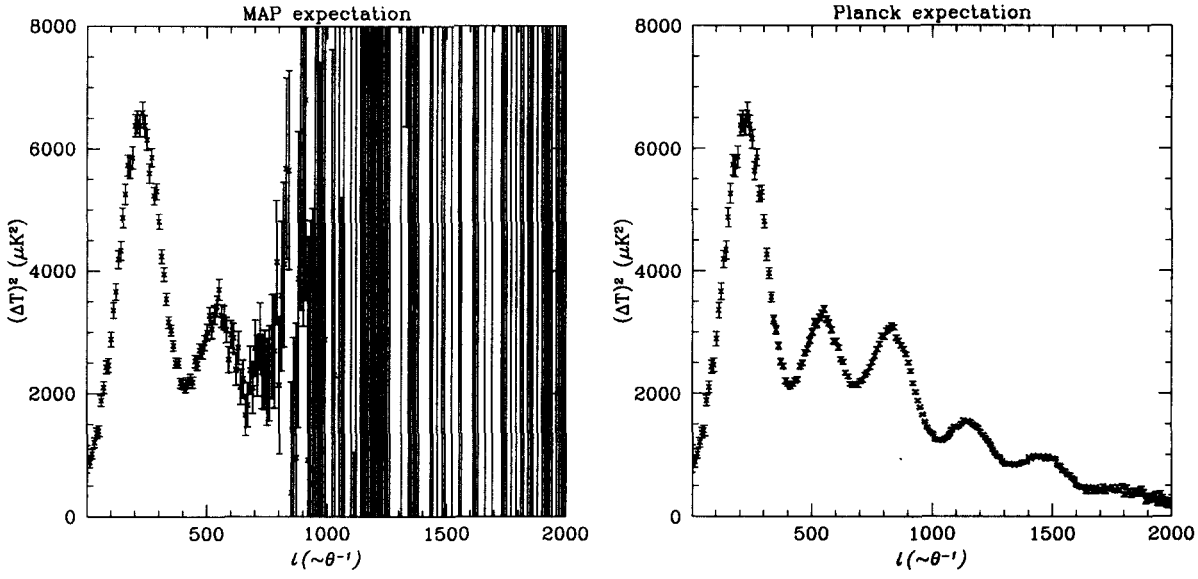

FIG 6.—Comparison of the expected uncertainties in the CMB power spectrum as determined by MAP, now flying, and Planck. At small values of ℓ, the uncertainty is dominated by statistical nature of a given realization of the underlying power spectrum (in other words, the Universe only provides so many independent samples at a given ℓ—this is often referred to as "cosmic variance"). For small ℓ, then, Planck will not improve on MAP. But above $\ell \approx 500$, the sensitivity and angular resolution of MAP start to dominate. Planck is designed to be limited by cosmic variance out to $\ell \approx 2000$, well into the region where the CMB anisotropy becomes very small and contains little additional information.

The solid line in Figure 7 shows a spatially flat model with parameters $\Omega_{\rm k} = 0$, $\Omega_\Lambda = 0$, $\omega_{\rm b} = 0.0125$, $\omega_{\rm cdm} = 0.2375$, $n_s = 1$, $n_t = 0$, and $r_2 = 0.2$. The dotted line shows another model with different parameters,

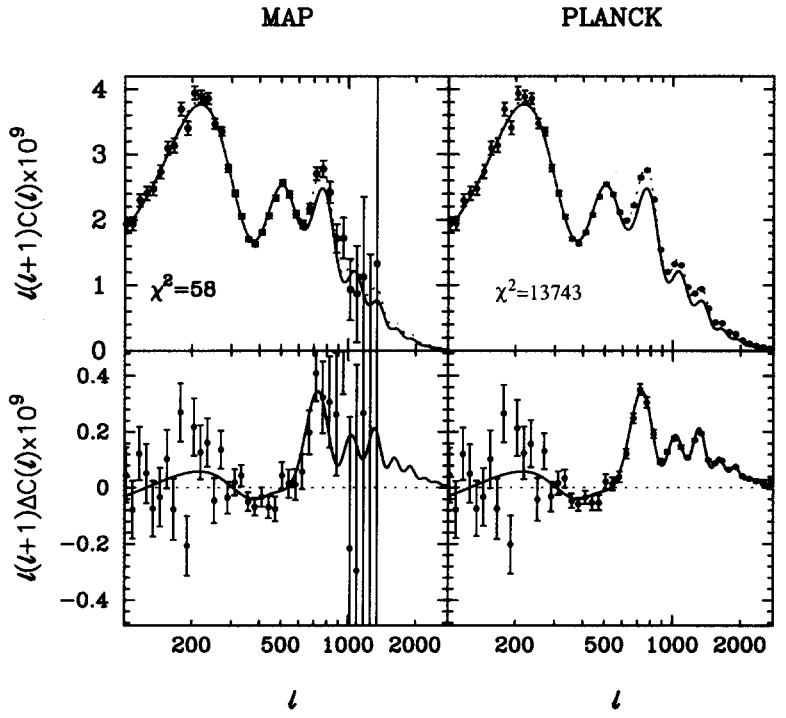

FIG 7.—Illustration of degeneracies amongst cosmological parameters. Power spectra for two almost degenerate CDM cosmological models with different parameters are plotted in the upper panels and the residuals are plotted in the lower panels. The error bars show simulated power spectra with the experimental sensitivities of MAP and Planck (see text for details). Although the baryonic density in the two models differs by 24%, and the CDM density differs by 5%, the two models are barely distinguishable by MAP, but easily distinguishable by Planck.

chosen specifically to produce an almost identical power spectrum. In fact, the power spectra of the two models are so nearly identical that they are difficult to discern in the upper panels. To show the differences, the lower panels show the residuals $\ell(\ell+1)\Delta C_\ell$ on an expanded scale. One can see immediately from the figure that for MAP the errors on C_ℓ become large at $\ell \gtrsim 700$, whereas Planck has been designed to produce near-cosmic-variance-limited measurements of the CMB temperature power spectra to high multipoles well into the damping tail of the CMB anisotropies ($\ell \gtrsim 2500$). In this example, the largest parameter change is a 24% change in the baryon density. This change is undetectable with a balloon experiment like Boomerang, marginally detectable by MAP, but easily detectable by Planck.†

Figure 8 compares MAP and Planck in a way that shows the effects of sensitivity and angular resolution separately. A family of *solid* curves shows (for a given cosmological model) the level of fluctuations that would be measured at infinite resolution (i.e., 0′ beams), and with the Planck beam from 30–217 GHz. The beam sizes

† One might ask how this result can be reconciled with the recent claims that the Boomerang/Maxima/DASI results already constraint ω_b to a precision of about 20%. The answer is that the accuracy of the determination of cosmological parameters is extremely sensitive to the *assumptions that are made in the analysis.* An extreme example is the *geometrical degeneracy*[e.g., 18], namely that two models with identical primordial fluctuation spectra, matter densities, and angular diameter distances to the last scattering surface will have identical CMB power spectra at multipoles $\ell \gtrsim 20$. As a consequence of the geometrical degeneracy, CMB experiments can produce accurate measurements of the curvature of the Universe Ω_k (if it is assumed that the fluctuations constitute either a pure adiabatic or isocurvature mode), but cannot distinguish between the total matter density ($\Omega_m = \Omega_b + \Omega_{cdm}$) and a cosmological constant (Ω_Λ). For all practical purposes, the geometrical degeneracy in linear perturbation theory is exact and can be removed only by invoking other constraints on the geometry of the Universe (e.g., as derived from Type Ia supernovae), observations of galaxy clustering, measurements of the Hubble constant, or from the effects of gravitational lensing on the CMB.

are used as labels. The beam sizes are effective sizes on the sky, taking into account (at least to first order) the effects of asymmetries and beam-smearing due to scanning rates and integration times. The larger the beam size, the less power would be measured at high multipoles. Three families of *dashed* curves show the 1σ noise expected for LFI, HFI, and MAP for mission lengths as specified. The "power" and "noise" curves of a given color cross at the ℓ value for which SNR = 1. Multipoles to the left of this point are well-determined, those to the right are not. It is clear that even a highly extended MAP mission cannot measure much beyond the second acoustic peak in the power spectrum, while LFI can measure past the third peak, and HFI can measure five or more peaks.

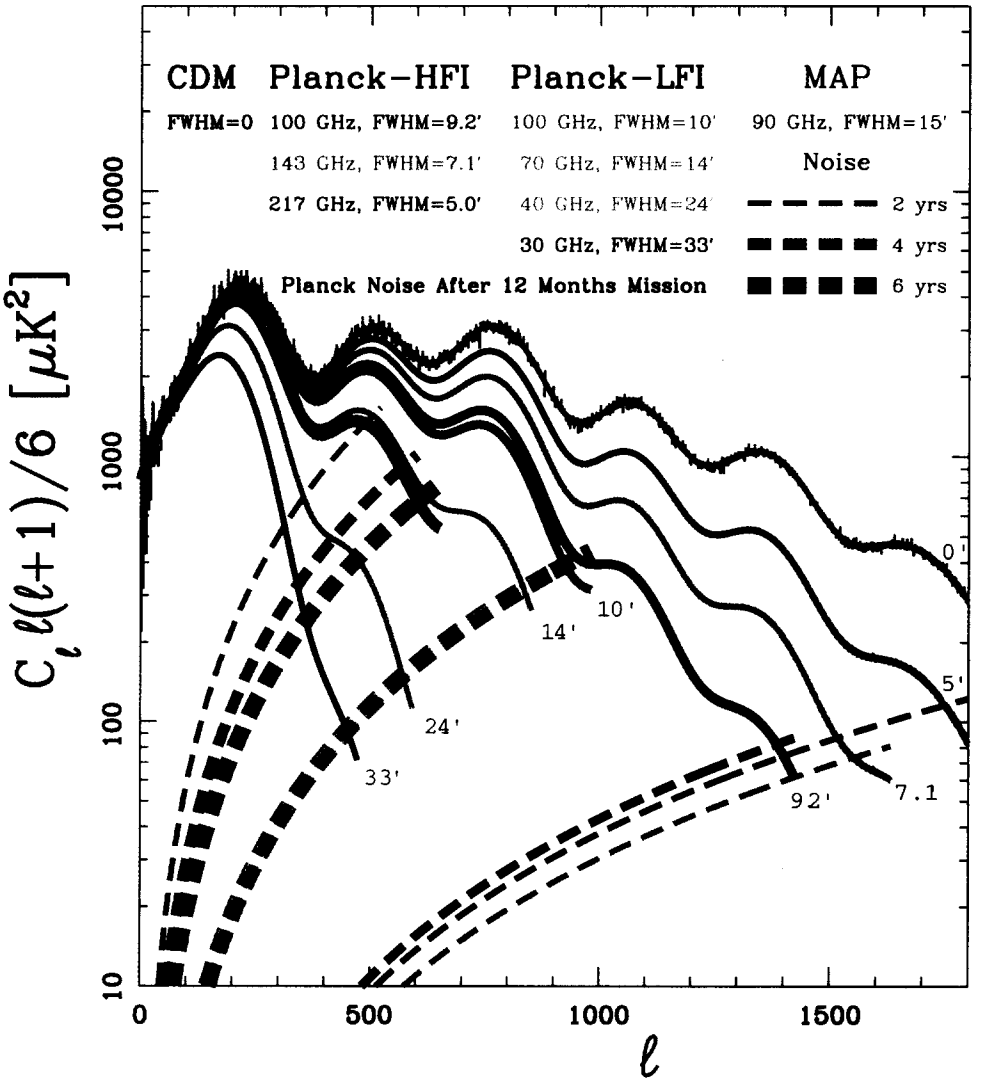

FIG 8.—Comparison of the expected performance of Planck and MAP that shows the effects of angular resolution and sensitivity on the multipoles that can be measured with signal-to-noise ratio greater than unity. See text for details. The four LFI noise curves by design (and some luck) lie atop each other, and are distinguished by color, linewidth, and endpoint.

All of these comparisons have been made on the basis of theoretical sensitivities expected for MAP and Planck. They do not take into account the effects of imperfect separation of confusing foregrounds, or of any other systematic errors. (For example, the HFI results in Figure 8 could be achieved in practice only with nearly perfect foreground removal. This requires a combination of LFI and HFI data, so the curves might more properly be labeled "Planck HFI+LFI".) And theoretical sensitivities before launch are certainly not guaranteed for any

mission! Put another way, the comparisons are meant to be "fair", but are not "real." They give insight into the design characteristics of the two missions, but they should not be taken as predictions of precisely what will be seen on orbit. The actual on-orbit performance of MAP is now known to the MAP team, but will not be released publicly for some months, while the actual on-orbit performance of Planck will not be known for many years to come.

CMB polarization has not yet been detected. So-called electric or E-type polarization is a firm prediction of inflationary models, resulting from Thomson scattering of quadrupole anisotropies in the surface of last scattering. However, detection of polarization is difficult, since the expected E-polarization anisotropies are much weaker than the temperature anisotropies. MAP and ground and balloon experiments will detect polarization well before Planck, but will barely make detections in a few bands around $l = 400$. Planck, on the other hand, should be able to map out C_l^E on all scales up to and beyond the (global) maximum at $l \sim 1000$ (set by the angle subtended by the photon mean free path at recombination). Critically, Planck should be able to detect the large-angle polarization signal, visible in Figure 9 that arises from the epoch of reionisation. The height of the peak at $\ell \sim 150$ provides valuable information on the optical depth to reionisation, and in models with abrupt reionisation the position of the peak can be used to constrain the reionisation epoch. The ability of large-angle polarization observations to measure independently the optical depth to reionisation breaks important degeneracies present in temperature-only measurements. For example, increasing the amplitude of the tensor modes relative to the scalars, and renormalising the combined spectrum, mimics the effects of increasing the optical depth. This degeneracy is broken very effectively with sensitive, large-angle polarization observations.

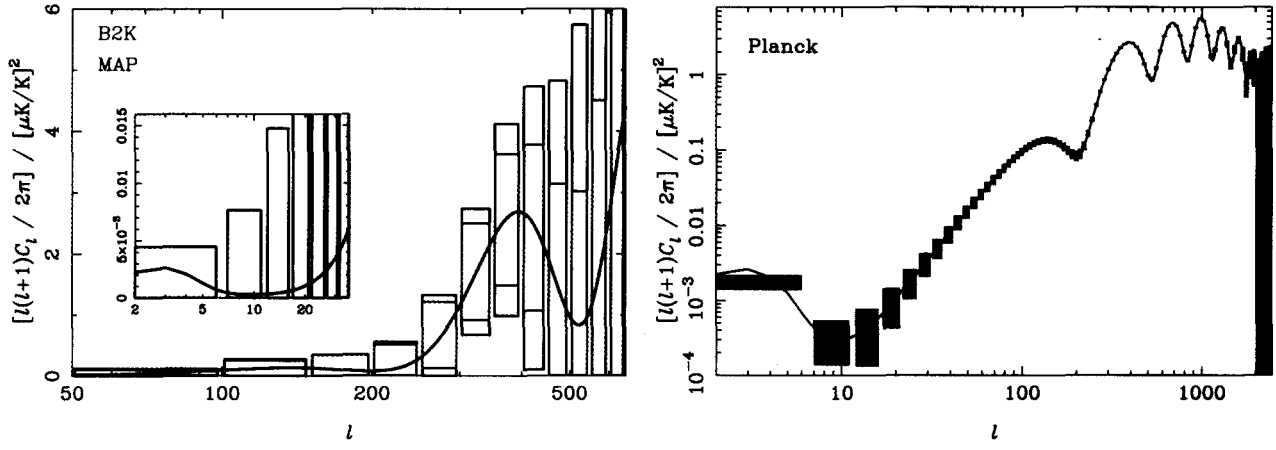

FIG 9.—Projections for the 1σ errors on the electric polarization power spectrum C_l^E from MAP and BOOMERanG2K (left) and Planck (right). In the left-hand plot, flat band powers are estimated with $\Delta_l = 50$ for both experiments for ease of comparison. Below $l = 50$ a finer banding has been adopted for MAP with the error estimates shown in the inset. The solid lines are the power spectrum C_l^X for a flat, adiabatic model with density parameters $\Omega_\Lambda = 0.7$, $\omega_b = 0.022$, $\omega_{cdm} = 0.12$, tensor quadrupole to scalar quadrupole ratio $r_2 = 0.2$, and an optical depth to reionisation of $\tau = 0.04$.

4. ALL-SKY SURVEYS

Planck is designed to measure the anisotropies of the CMB, but to do that it will produce the most sensitive all-sky surveys ever made at frequencies from 30 to 857 GHz. The previous all-sky surveys in this frequency range are those of MAP (22–90 GHz) now underway, and COBE FIRAS. Planck's sensitivity to compact sources will be roughly an order of magnitude better than MAP's, a result of both lower noise and better angular resolution, and many orders of magnitude better than FIRAS', which had a single detector and 7° angular resolution. In a real sense, Planck will produce the first submillimeter all-sky surveys useful for compact sources (see Table 1 for source sensitivities).

Because so little is known about the detailed characteristics of discrete sources in this frequency range,

predictions of the number of sources that Planck will detect are highly uncertain. Nevertheless, estimates suggest that something like 2,000 extragalactic radio sources will be detected, and something like 10^4 dusty galaxies. Source counts are known to be steep in the flux density ranges relevant for Planck, so the numbers will be much larger than for previous surveys. In any event, Planck will find *all* of the brightest and rarest sources in the sky, thereby significantly advancing studies of the tip of the luminosity function for all classes of source, and providing a unique catalog of objects for follow-up with instruments such as Herschel and ALMA. A question of particular interest that Planck will address is to what extent the tip of the AGN luminosity function is dominated by gravitational lensing.

In addition, through the Sunyaev-Zel'dovich effect Planck should detect about 10,000 galaxy clusters, including every cluster that can be detected by any past, present, or planned X-ray mission. Both the kinetic and thermal SZ effects will be measured. Planck's resolution is not ideal for SZ studies, but the unbiased all-sky catalog that it produces will support extensive follow-up observations at higher resolution, and the combination with X-ray data on the same clusters will be powerful. Planck's measurements of the thermal SZ effect the cluster radial velocities derived from it will be limited by its angular resolution and the intrinsic CMB anisotropies underlying the cluster; however, by combining the results from many clusters in the same part of the sky, determination of radial velocities for super-cluster masses should be possible to $100\,\mathrm{km\,s^{-1}}$ or so.

Important data will be obtained on the diffuse emission from the Milky Way as well. Dust, free-free, and synchrotron emission will all be measured. Polarization data will enable studies of the Galactic magnetic field, on both small and large angular scales.

5. SUMMARY

The CMB is the most important source of information about the content and geometry of the Universe that we have. With large arrays of state-of-the-art cryogenic detectors, supported by a pathbreaking set of mechanical coolers, Planck is designed to measure the temperature anisotropies of the CMB to fundamental limits imposed by the Universe itself, on angular scales down to 5′. In addition, it will make breakthrough measurements of the polarization of the CMB, and provide all-sky surveys whose legacy may well last as long as that of IRAS.

ACKNOWLEDGMENTS

Much of the material in this contribution is adapted from a document entitled *The Scientific Programme of Planck*, in preparation by the Planck Science team, edited by George Efstathiou and me in our roles as HFI and LFI Survey Scientists, respectively, and to be published in the coming year by the European Space Agency. I would like to thank especially: Jan Tauber, Planck Project Scientist, for some of the material in Section 1, and Figures 1 and 2; George Efstathiou, for material in Section 2, and Figures 7 and 9; and Kris Gorski, for Figure 8.

REFERENCES

1. N. Mandolesi. "Low-frequency instrument of Planck," in *IR Space Telescopes and Instruments*, this volume.
2. M. Lamarre. "Planck high-frequency instrument," in *IR Space Telescopes and Instruments*, this volume.
3. M. Piat and J. M. Lamarre. "Planck-HFI thermal architecture: from requirements to solutions," in *IR Space Telescopes and Instruments*, this volume.
4. J. B. Riti, E. Gavilla, and B. Guillaume. "Planck payload module design and performance," in *IR Space Telescopes and Instruments*, this volume.
5. T. de Graauw, T. G. Phillips, J. Stutzki, and N. D. Whyborn. "Herschel heterodyne instrument for the far-infrared (HIFI): overview and development," in *IR Space Telescopes and Instruments*, this volume.
6. J. C. Pearson et al. "THz frequency receiver instrumentation for Herschel's heterodyne instrument for the far-infrared (HIFI)," in *IR Space Telescopes and Instruments*, this volume.
7. T. Klein et al. "Local oscillator unit for Herschel/HIFI," in *IR Space Telescopes and Instruments*, this volume.
8. A. Poglitsch, C. Waelkens, and A. N. Geis. "Herschel photodetector array camera and spectrometer (PACS)," in *IR Space Telescopes and Instruments*, this volume.

9. R. Graue, D. Kampf, and A. Poglitsch. "Herschel PACS focal plane unit," in *IR Space Telescopes and Instruments*, this volume.
10. M. J. Griffin, B. M. Swinyard, and L. G. Vigroux. "SPIRE: Herschel's submillimeter camera and spectrometer," in *IR Space Telescopes and Instruments*, this volume.
11. B. M. Swinyard et al. "Imaging FTS for Herschel SPIRE," in *IR Space Telescopes and Instruments*, this volume.
12. D. B. Gallagher, W. R. Irace, and M. W. Werner. "SIRTF mission," in *IR Space Telescopes and Instruments*, this volume.
13. R. A. Hopkins, R. B. Schweickart, and S. M. Volz, "Cryogenic/thermal system for the SIRTF cryogenic telescope assembly," in *IR Space Telescopes and Instruments*, this volume.
14. P. T. Finley, R. L. Oonk, and R. B. Schweickart, "Thermal performance verification of the SIRTF cryogenic telescope assembly," in *IR Space Telescopes and Instruments*, this volume.
15. R. K. Sachs & A. M. Wolfe (1967), "Perturbations of a Cosmological Model and Angular Variations of the Microwave Background," ApJ, 147, 73.
16. G. F. Smoot et al. 1992, "Structure in the COBE differential microwave radiometer first-year maps," ApJLett, 396, L1.
17. Sievers *et al.*. "Cosmological Parameters from Cosmic Background Imager Observations and Comparisons with BOOMERANG, DASI, & MAXIMA," ApJ submitted astro-ph/025387 23 May 2002.
18. J. R. Bond, G. Efstathiou, & M. Tegamrk 1997, "Forecasting cosmic parameter errors from microwave background anisotropy experiments," MNRAS, 291, L33.